Engineering Analysis with Boundary Elements 72 (2016) 65–77

Contents lists available at ScienceDirect

Engineering Analysis with Boundary Elements

journal homepage: www.elsevier.com/locate/enganabound

Three-dimensional fracture propagation with numerical manifold method

Yongtao Yang [a], Xuhai Tang [b,*], Hong Zheng [c], Quansheng Liu [b], Lei He [d]

[a] State Key Laboratory of Geomechanics and Geotechnical Engineering, Institute of Rock and Soil Mechanics, Chinese Academy of Sciences, Wuhan, China
[b] School of Civil Engineering, Wuhan University, Wuhan, China
[c] Key Laboratory of Urban Security and Disaster Engineering, Ministry of Education, Beijing University of Technology, Beijing 100124, China
[d] School of Civil Engineering, Monash University, Australia

ARTICLE INFO

Article history:
Received 15 December 2015
Received in revised form
12 August 2016
Accepted 13 August 2016

Keywords:
Fracture propagation
Three dimensional simulation
Numerical manifold method (NMM)
Maximum tensile stress criterion

ABSTRACT

By introducing the concept of mathematical cover and physical cover, the numerical manifold method (NMM) is able to solve continuous and discontinuous problems in a unified way. In this paper, the NMM is developed to analyze three dimensional (3D) fracture propagation. The maximum tensile stress criterion is implemented to determine whether the fracture will propagate and the direction of fracture propagation. Three benchmark problems are analyzed to validate the present algorithm and program. The numerical results replicate available experimental results and existing numerical results. The present algorithm and 3D NMM code are promising for 3D fracture propagation. They deserve to be further developed for the analysis of rock mechanic problems in which the initiation and propagation of multiple fractures, tensile and shear fractures, and fracture propagation under compressive loading are taken into account.

1. Introduction

Analyzing the evolution of fractures in fractured rock mass is of great importance in many fields [1]. With the development of computer science, the numerical method has become one of the most effective approaches to understand fracture evolution, which attracts a great number of researchers during the last decade. Up to now, a great number of versatile numerical approaches have been proposed to simulate fractures, such as Finite Element Method (FEM) [2] with remeshing strategy, Boundary Element Method (BEM) [3] and meshfree methods [4].

Nowadays, Finite Element Method (FEM) [2] is the most widely used numerical approach in engineering and have been utilized to simulate three-dimensional (3D) fracture propagation for several decades. However, it still suffers from the significant difficulties in mesh generation and refinement during fracture simulation. In FEM, fracture surfaces must coincide with the element boundaries, therefore the meshes must be updated at each simulation step. Additionally, the meshes are required to be more refined in the vicinity of fracture tips than in the remainder of the model, in order to obtain sufficiently accurate solution for the fracture analysis [5]. Especially, when the problems are taken into account in 3D, the simulations are significantly more difficult. Polygonal Finite Element Method (PFEM) [6–8] is a development of FEM, which is able to construct proper approximations on polygonal elements, and provides an effective approach to remesh and refinement in two dimensions [9]. In order to model the development of arbitrary multiple fractures in 3D, Paluszny has developed a robust simulator using global remeshing strategy [10], which has been successfully utilized in investigating block caving system [11–13], oil recovery [14,15], and predicting the permeability of three-dimensional fractured porous rock [16]. However, global strategy is not suitable in some special problems. When the fractured zone is obviously smaller than the whole computational model, this global strategy is not cost-effective. Therefore, a number of methodologies are developed for introducing fractures into computational model without remeshing, including the numerical manifold method (NMM) which is developed in this work.

The Boundary Element Method (BEM) is an alternative approach to solve fracture propagation problems because it could reduce the dimensions of the problems and simplify the complexity [17]. In 2014, Wu and Olson [18] utilized BEM to study the simultaneous multiple fracture treatments in hydraulic fracturing. The main drawbacks of BEM are the difficulty to solve nonlinear problems [19] and the difficulty to handle computational models which contains many different materials.

Meshfree methods do not need a mesh to discretize the problem domain, and therefore are very suitable to solve complex

* Corresponding author.
E-mail address: xuhaitac@163.com (X. Tang).

http://dx.doi.org/10.1016/j.enganabound.2016.08.008
0955-7997/

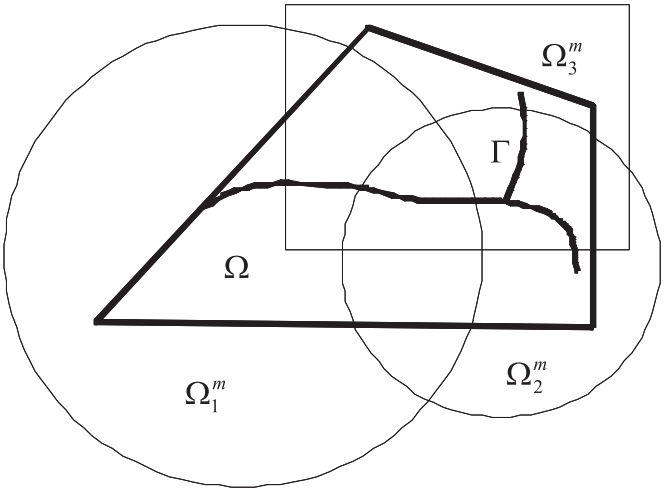

Fig. 1. Problem domain (thick lines) and mathematical cover (fine lines) [40].

practical problems such as large deformation [20] and fracture propagation simulation [21]. The main contributions to the development of meshfree methods are known in the literatures as Element-Free Galerkin method (EFG) [22], Reproducing Kernel Particle Method (RKPM) [23] and stable particle methods [24]. Bordas et al. [25] have shown that the high flexibility of meshfree methods can be exploited to model arbitrary three-dimensional fracture initiation, propagation, branching and junction in nonlinear materials. Nonetheless the high computational cost and complex process in constructing the trial functions will deteriorate the stability and efficiency of numerical integration [26]. Moreover, they cannot be implemented into existing finite element data structures [19].

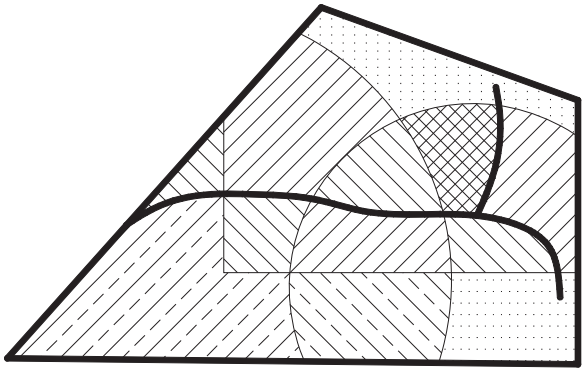

Fig. 3. Manifold elements from the PC [40].

In order to overcome the burden of meshing and remeshing of the FEM in modeling three-dimensional fracture problems, some Partition of Unity [27] based approaches have been developed, which can be considered as an improvement of FEM. Typical of them are the eXtended Finite Element Method (XFEM) [28,29] and generalized finite element method (GFEM) [19,30]. In XFEM, the generalized Heaviside functions and the asymptotic fracture-tip functions are incorporated into the FEM to account for the fractures, without the need for the finite element mesh to conform to the fractures [31]. In GFEM [30], the standard finite element spaces are augmented by adding special functions which reflect the known information about the boundary value problem and the input data to model problems with multiple straight reentrant corners, voids, and fractures.

In 1991, Shi [32] developed numerical manifold method (NMM) for geotechnical engineering, which also falls into the category of the partition of unity. The main attractive advantage of NMM is to

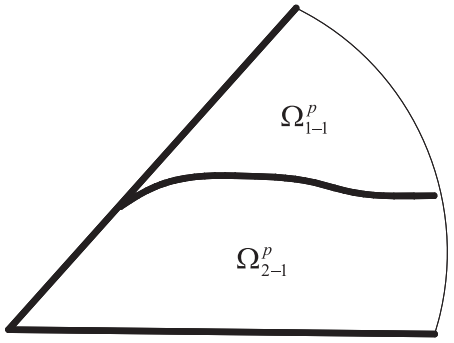

(a) Physical patches Ω_{1-1}^p and Ω_{2-1}^p generated from mathematical patch Ω_1^m

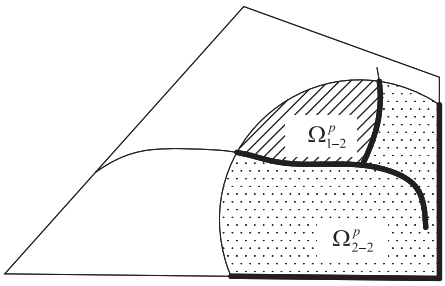

(b) Physical patches Ω_{1-2}^p and Ω_{2-2}^p generated from mathematical patch Ω_2^m

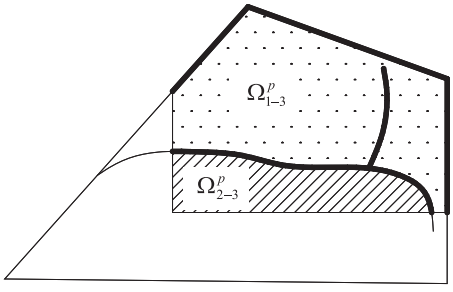

(c) Physical patches Ω_{1-3}^p and Ω_{2-3}^p generated from mathematical patch Ω_3^m

Fig. 2. Physical patches from mathematical patches [40], (a) Physical patches Ω_{1-1}^p and Ω_{2-1}^p generated from mathematical patch Ω_1^m (b) Physical patches Ω_{1-2}^p and Ω_{2-2}^p generated from mathematical patch Ω_2^m (c) Physical patches Ω_{1-3}^p and Ω_{2-3}^p generated from mathematical patch Ω_3^m.

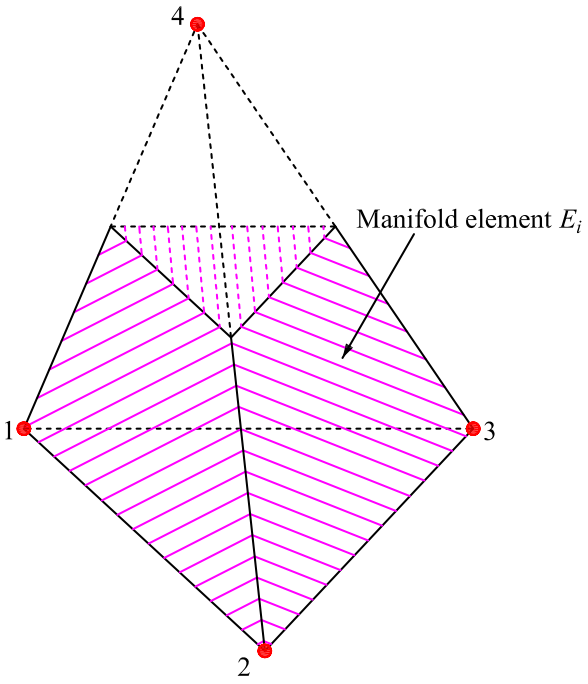

Fig. 4. A three-dimensional manifold element.

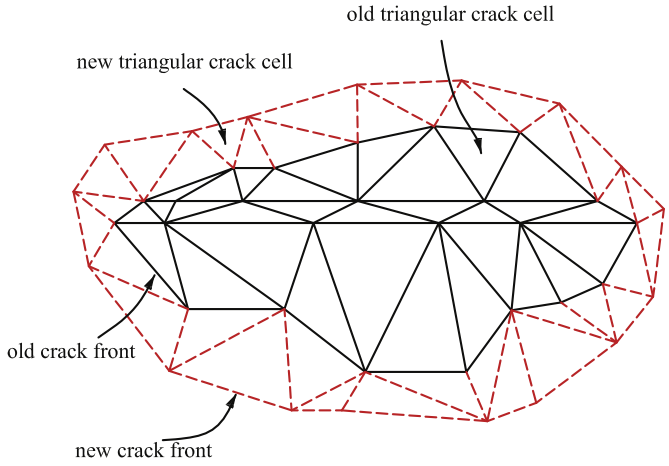

Fig. 5. Three-dimensional representation of fracture surface with triangular fracture cell.

simulate continuous and discontinuous problems in a unified way. NMM has been successfully applied to simulate fracture problems in many fields. Chiou et al. [33] captured the mixed mode fracture propagation trajectory by combining NMM with the virtual fracture extension method, as well as auto-remeshing schemes. Terada et al. [34] presented the finite cover method, alias of NMM, for

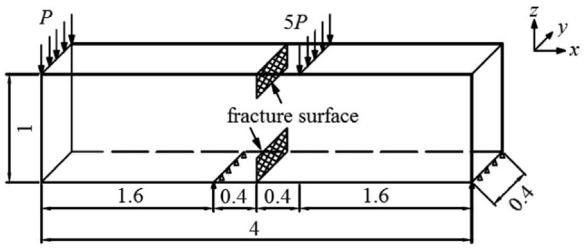

Fig. 7. Sketch of the beam under four-point loading.

progressive failure analyses with cohesive fracture zone in heterogeneous solids and structures. Zheng et al. [35] reduced the growth of multiple fractures to a nonlinear complementarity problem (NCP) and simulated the propagation process with MLS-based numerical manifold method. According to their report, some interesting and profound phenomena in brittle fracture are revealed. Ma and his coauthors [31,36] incorporated the concept of singular physical cover into the NMM to model complex fracture and fracture propagation problems. Ning et al. [37] adopted the Mohr-Coulomb criterion with a tensile cut-off, and successfully simulated the progressive failures of rock slopes, where frictional contact of fracture surfaces is involved. Wu et al. [38] numerically modeled and investigated the viscoelastic deformation behavior of a sedimentary rock under different loading rates by incorporating a modified 3-element viscoelastic constitutive mode in the NMM. Zhang et al. [39] solved thermo-mechanical fracture of planar solids problems with NMM, where the singularity of temperature as well as displacement is reflected.

Although various fracture problems were solved by the NMM, the previous work was limited in two-dimensional problems. In this study, as a preliminary exploration in the discontinuity modeling, the NMM is extended to investigate 3D fracture propagation of isotropic homogeneous materials. The outline of this paper is as follows: in Section 2, the basic concept of NMM is briefly introduced; Section 3 presents technique associated with 3D fracture propagation, such as fracturing algorithm and fracture tracking in great detail. Several numerical examples are presented in Section 4. Some conclusions are drawn in the last section.

2. Brief introduction to NMM

2.1. Basic concepts of NMM

In order to simulate continuous and discontinuous problems in a unified way, two cover systems, namely, the mathematical cover (MC) and the physical cover (PC) have been introduced into NMM. In this section, the basic concept of NMM is briefly introduced, more details can be found in [40,41].

The MC is composed of a series of mathematical patches (MPs), Ω_i^m, ($i = 1, \ldots, n^m$). Here, n^m is the number of all MPs. Different MPs

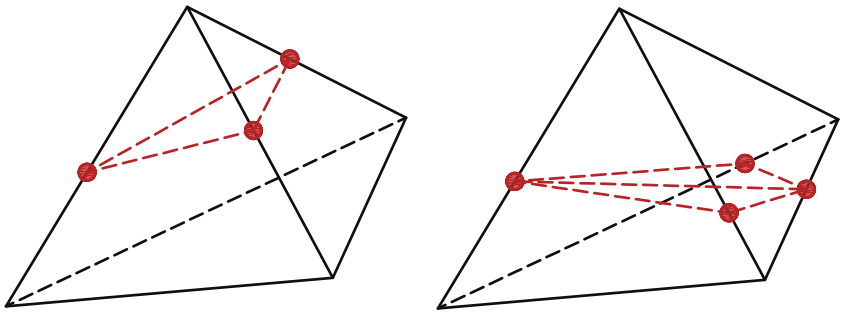

Fig. 6. An example to illustrate manifold element update during fracturing process.

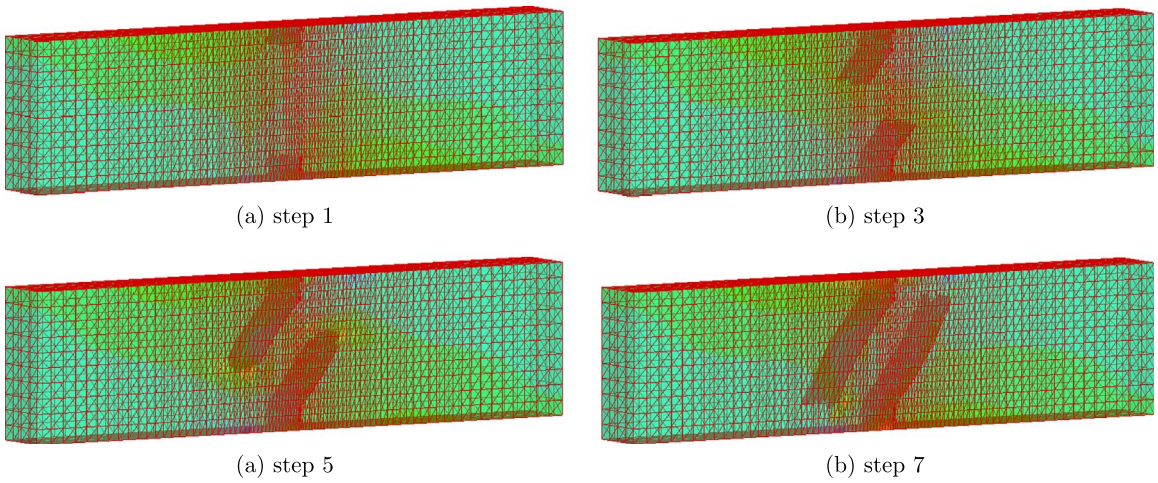

Fig. 8. Fracture propagation within the beam under four-point loading obtained using 3D NMM.

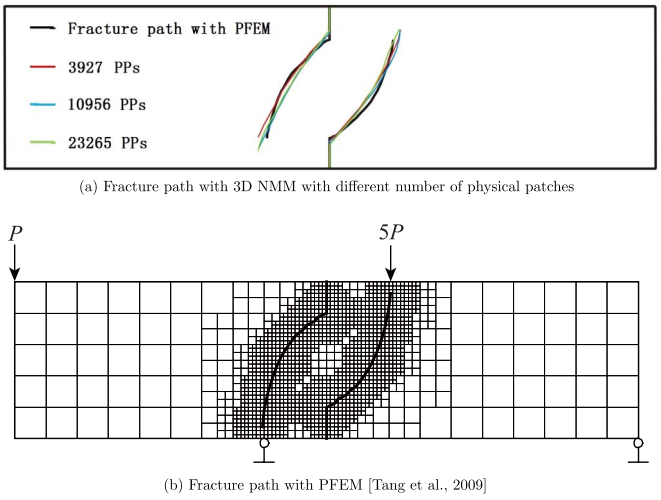

Fig. 9. The comparison of fracture paths within the beam under four-point loading obtained using 3D NMM and Polygonal Finite Element Method (PFEM), (a) Fracture path with 3D NMM with different number of physical patches (b) Fracture path with PFEM [9].

can partially overlap each other. The only requirement for MC is able to cover the entire problem region Ω.

Associated with each MP Ω_i^m, there is a weight function, $w_i(\mathbf{r})$ ($i = 1, \ldots, n^m$), with $\mathbf{r}$ the position vector, satisfying the following properties

$$\begin{aligned} &w_i(\mathbf{r}) = 0, \quad \text{if } \mathbf{r} \notin \Omega_i^m \\ &0 \le w_i(\mathbf{r}) \le 1, \quad \text{if } \mathbf{r} \in \Omega_i^m \\ &\sum_{i=1}^{n^m} w_i(\mathbf{r}) = 1, \quad \text{if } \mathbf{r} \in \Omega_i^m \end{aligned} \tag{1}$$

$w_i(\mathbf{r})$ is collectively called the partition of unity subordinating to $\{\Omega_i^m\}$.

As shown in Fig. 1, the computational domain Ω containing a bifurcation fracture Γ with two fracture tips are covered by three MPs, i.e., Ω_1^m - the bigger circle, Ω_2^m - the smaller circle, and Ω_3^m - the rectangle.

By cutting all the mathematical patches $\{\Omega_i^m\}_1^3$, one by one, with the components of Ω, including the boundary, the material interface and the fracture, the physical patches (PPs) are generated, as shown in Fig. 2. From one mathematical patch Ω_i^m, more than one smaller domain might be created. We represent these smaller

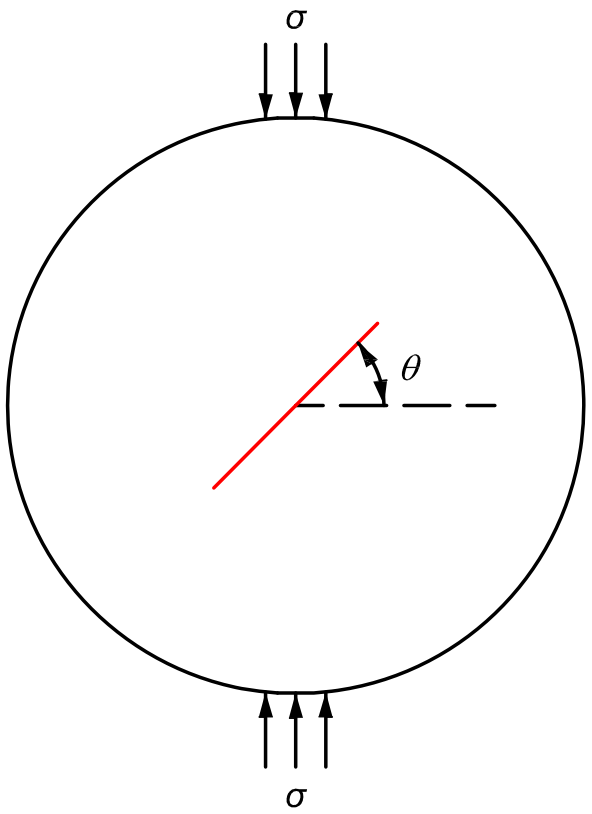

Fig. 10. The geometry and boundary conditions of the pre-notched disc.

domains by Ω_{j-i}^p, ($j = 1, \ldots, n_i^p$) with Ω_{j-i}^p called the j-th physical patch created from the mathematical patch Ω_i^m. Here, n_i^p is the number of all physical patches that are all created from the same mathematical patch Ω_i^m. The union of all Ω_{j-i}^p,

$$\cup_{i=1}^{m} \cup_{j=1}^{n_i^p} \Omega_{j-i}^p \tag{2}$$

is named as physical cover (PC) and accordingly match Ω exactly.

Each physical patch Ω_{j-i}^p contains the local geometric features of the problem domain and can be assigned other given information. For example, Ω_{2-2}^p contains the fracture tip of fracture Γ (see Fig. 2 (b)).

According to the geometric and mechanical features of Ω_{j-i}^p, one can construct a good enough local approximation $\mathbf{u}_{j-i}(\mathbf{r})$ over Ω_{j-i}^p to reflect the known information about the boundary value

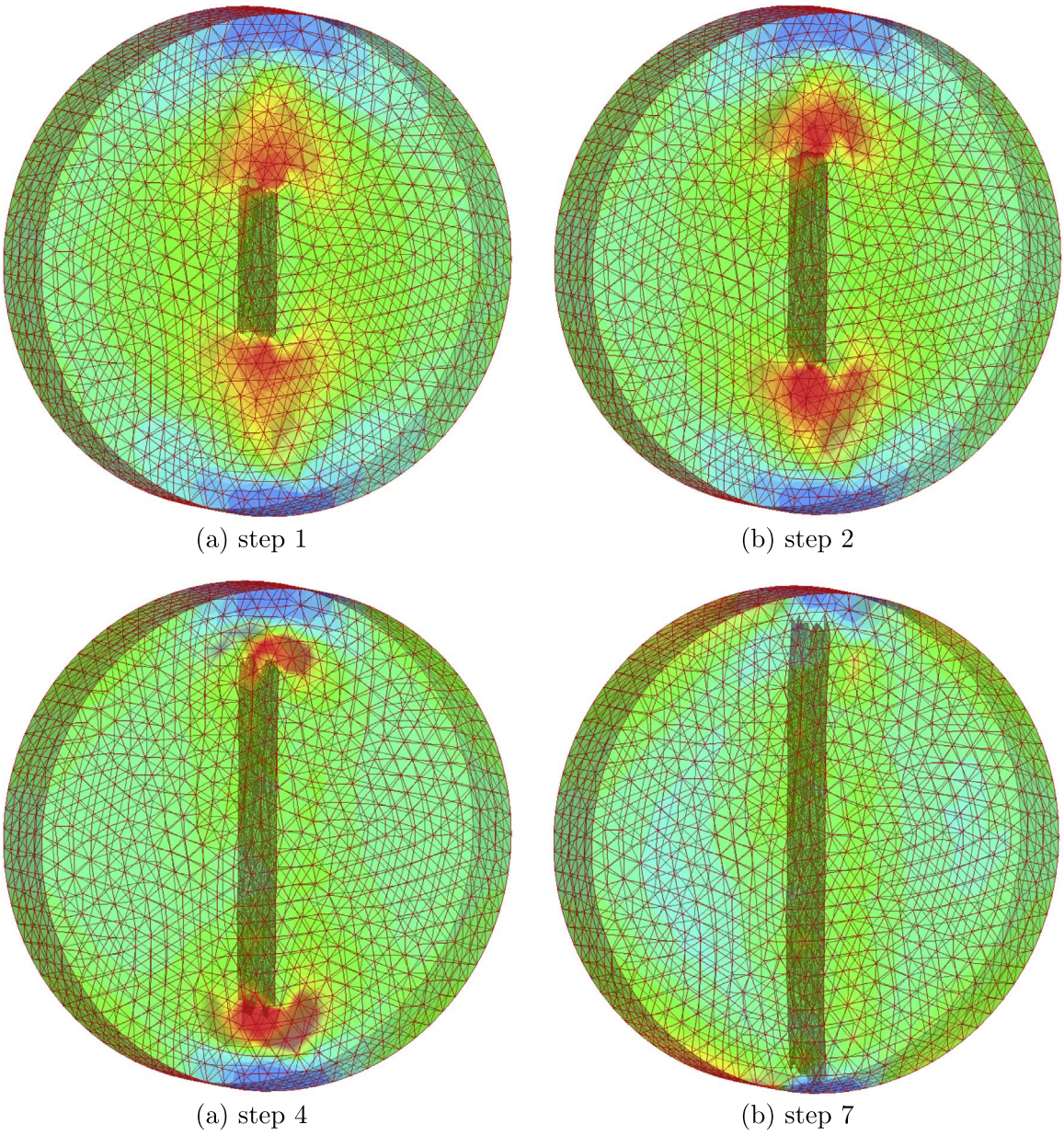

Fig. 11. Fracture path within pre-notched disc obtained by 3D NMM ($\theta = 90°$).

problem and the input data to model the problem. The formulation of $\mathbf{u}_{j-i}(\mathbf{r})$ could be expressed as

$$\mathbf{u}_{j-i}(\mathbf{r}) = \mathbf{T}_{j-i}(\mathbf{r})\mathbf{d}_{j-i},\ \mathbf{r} \in \Omega^p_{j-i} \tag{3}$$

where, vector $\mathbf{d}_{j-i}$ is composed of the degrees of freedom for physical patch Ω^p_{j-i}, and $\mathbf{T}_{j-i}(\mathbf{r})$ is composed of some given functions which could reflect the local behaviors of the solution over Ω^p_{j-i}, see details in [40].

By restricting $w_i(\mathbf{r})$ defined on Ω^m_i onto Ω^p_{j-i}, $(j = 1, \ldots, n^p_i)$, the weight function $w_{j-i}(\mathbf{r})$ subordinate to Ω^p_{j-i} is obtained. $w_{j-i}(\mathbf{r})$, $(j = 1, \ldots, n^p_i)$, might have the same expression as $w_{j-i}(\mathbf{r})$, but they have totally different domains of definition, corresponding to $\Omega_{j-i}(\mathbf{r})$, $(j = 1,..., n^p_i)$, respectively, which all come from the same mathematical patch Ω^m_i. Besides, different local approximation $\mathbf{u}_{j-i}(\mathbf{r})$ are defined over each Ω^p_{j-i}. This enables NMM to simulate discontinuity across the common boundaries between physical patches.

For simplicity of presentation, all Ω^p_{j-i}, $w_{j-i}(\mathbf{r})$ and $\mathbf{u}_{j-i}(\mathbf{r})$ are coded with a single subscript and represented by Ω^p_k, $w_k(\mathbf{r})$ and $\mathbf{u}_k(\mathbf{r})$, $(k = 1, \ldots, n^p)$, respectively. Here, n^p is the number of all the physical patches, and defined as

$$n^p = \sum_{i=1}^{n^m} n^p_i \tag{4}$$

In conventional NMM, a manifold element, basic unit in integrating the weak formulation of the problem, is a common domain of as many as possible physical patches and denoted by E_i in the present paper. Fig. 3 displays all the twelve numerical manifold elements generated from the MC shown in Fig. 1.

Then, the global approximation $\mathbf{u}(\mathbf{r})$ in a manifold element E_i could be obtained by adding all the local approximations multiplied by the weight functions

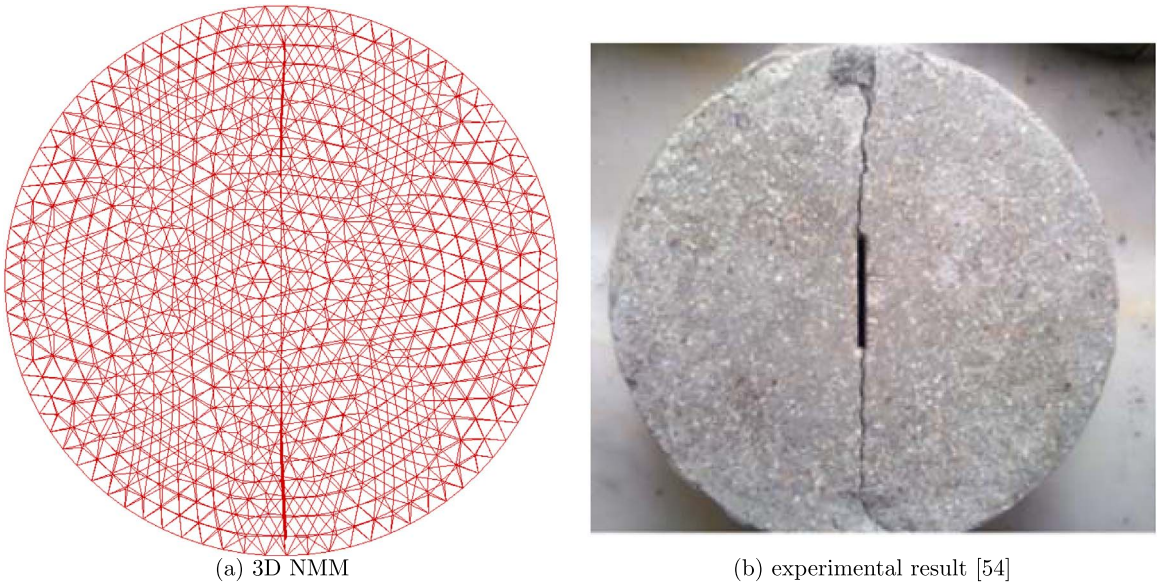

(a) 3D NMM (b) experimental result [54]

Fig. 12. The comparison between numerical simulation and experimental results for the fracture path of pre-notched disc ($\theta = 90°$), (a) 3D NMM (b) experimental result [54].

$$\mathbf{u}(\mathbf{r}) = \sum_{k=1}^{n^p} w_k(\mathbf{r})\mathbf{u}_k(\mathbf{r}),\ \mathbf{r} \in E_i \tag{5}$$

Theoretically, the MC can be constructed arbitrarily. Up to now, however, for the simplicity of implementation, almost all the applications and developments of NMM have selected finite element meshes to construct the MC. The mesh, which is independent neither the internal discontinuities nor the external boundary, is referred to as the mathematical mesh.

In regard to 2D case, it is best to choose regular meshes (equilateral triangular or rectangular mesh) as the mathematical mesh for the consideration of accuracy. If triangular mesh is used, all the triangles around one node form one mathematical patch. If rectangular mesh is used, all the rectangles around one node form one mathematical patch.

2.2. Framework of 3D NMM

Considering 3D NMM, we can choose the tetrahedral mesh to form the mathematic cover which should cover the entire problem region Ω. All the tetrahedrons around one node form one mathematical patch. By cutting the mathematical patches one after another with the components of the problem domain, including the domain boundaries, the material interfaces, and the discontinuities, the physical patches (PPs) are generated. A manifold element is the common part of four PPs. Four PPs can be regarded as four generalized nodes of the manifold element (Fig. 4).

Then, the global approximation $\mathbf{u}(x, y, z)$ in a manifold element E_i in Eq. (5) could be rewritten as

$$\mathbf{u}(x, y, z) = \sum_{k=1}^{4} w_k(x, y, z)\mathbf{u}_k(x, y, z),\ (x, y, z) \in E_i \tag{6}$$

The weight functions in Eq. (6) take the form of

$$\begin{Bmatrix} w_1(\mathbf{r}) \\ w_2(\mathbf{r}) \\ w_3(\mathbf{r}) \\ w_4(\mathbf{r}) \end{Bmatrix} = \begin{bmatrix} f_{11} & f_{12} & f_{13} & f_{14} \\ f_{21} & f_{22} & f_{23} & f_{24} \\ f_{31} & f_{32} & f_{33} & f_{34} \\ f_{41} & f_{42} & f_{43} & f_{44} \end{bmatrix} \begin{Bmatrix} 1 \\ x \\ y \\ z \end{Bmatrix} = \mathbf{W1}(x, y, z) \tag{7}$$

in which

$$\mathbf{W} = \begin{bmatrix} f_{11} & f_{12} & f_{13} & f_{14} \\ f_{21} & f_{22} & f_{23} & f_{24} \\ f_{31} & f_{32} & f_{33} & f_{34} \\ f_{41} & f_{42} & f_{43} & f_{44} \end{bmatrix} = \frac{1}{\Delta} \begin{bmatrix} A_{11} & -A_{12} & A_{13} & -A_{14} \\ -A_{21} & A_{22} & -A_{23} & A_{24} \\ A_{31} & -A_{32} & A_{33} & -A_{34} \\ -A_{41} & A_{42} & -A_{43} & A_{44} \end{bmatrix} \tag{8}$$

$$\Delta = \begin{bmatrix} 1 & x_1 & y_1 & z_1 \\ 1 & x_2 & y_2 & z_2 \\ 1 & x_3 & y_3 & z_3 \\ 1 & x_4 & y_4 & z_4 \end{bmatrix} \tag{9}$$

A_{ij} is algebraic component of Δ.

In general, the local approximations $\mathbf{u}_k(x, y, z)$ defined on one physical patch can be constant, linear or higher-order polynomials [42]. In this study, the local approximations are taken as constants for simplicity and avoiding the "linear dependence problems" [43,44], although the higher-order polynomial terms enable us to improve the accuracy of approximation.

Moreover, as discussed in the previous text, special functions which reflect the known information about the boundary value problem could be added into the local approximations to augment the finite element spaces. Zheng et al. [40] have successfully added the first two items of Williams' series [45] into the local approximations of the singular patches to tackle partially fractureed elements and fracture tip singularities. However, such a treatment will subsequently complicate the computation including the inheritance of the degrees of freedom and initial stress for dynamic problems, deploying special Gauss integration scheme for fracture tip elements and dilute the ability to undertake integration explicitly [37]. It is especially computational expensive when dealing with rock engineering problems which may involve hundreds or even thousands of fractures within the problem domain. In the present work, instead of adding the first two items of Williams' series into the local approximations for the singular patches, we regulate the fracture front stop at element boundaries to avoid partially fractureed elements. Evidently, as discussed in [37], this approach yields a degree of inaccuracy for a coarse mesh. However, accuracy could be improved by adopting a finer discrete model.

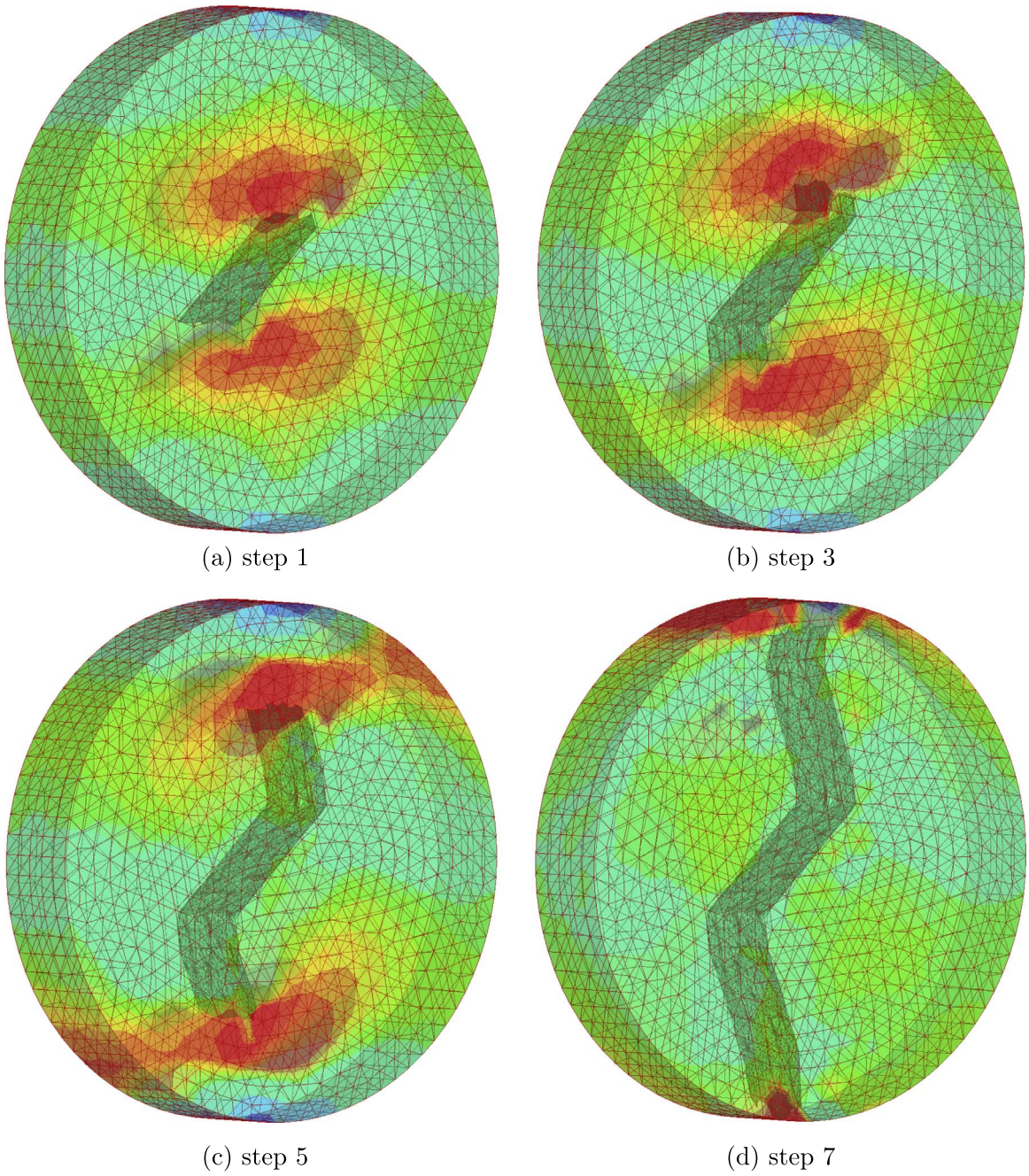

Fig. 13. Fracture path within pre-notched disc for various steps obtained by 3D NMM .

It is known that regular hexahedral mesh can be employed to construct the MC of 3D NMM. However, as mentioned in [41], an assemblage of regular tetrahedral mesh fails to completely fill the 3D space. Although tetrahedral mesh is possible through dividing each hexahedron in a regular hexahedral mesh into several tetrahedrons, this will not be able to obtain the tetrahedral mesh with optimal topological shape.

In this paper, for the simplicity of implementation, tetrahedral mesh generated by ABAQUS is employed to construct the MC within the problem domain without considering the fractures, which means the mathematical mesh will coincide with the material boundary. Then the fractures are deployed, followed by a series of cutting operations discussed in great detail in [46] to generate physical cover and manifold elements.

It is noted that, for our 3D NMM, mathematical cover only needs to match the material boundary of problem domain, but do not have to match the fractures, which is a significant advantage over the FEM. Moreover, in the simulation of fracture propagation, our 3D NMM can avoid the remeshing process which is another important advantage over the FEM.

3. Numerical manifold method for 3D fracture propagation

The NMM is able to simulate continuous and discontinuous problems in a unified way. Before applying it to simulate the transition from continuum to discontinuum, a robust and easy implementing fracture algorithm should be developed. In the past decades, the fracture mechanics has been widely used and shown its validity and accuracy through many benchmark problems. However, fracture mechanics cannot deal with the initiation of new fractures, because fracture mechanics is built for pre-cracked

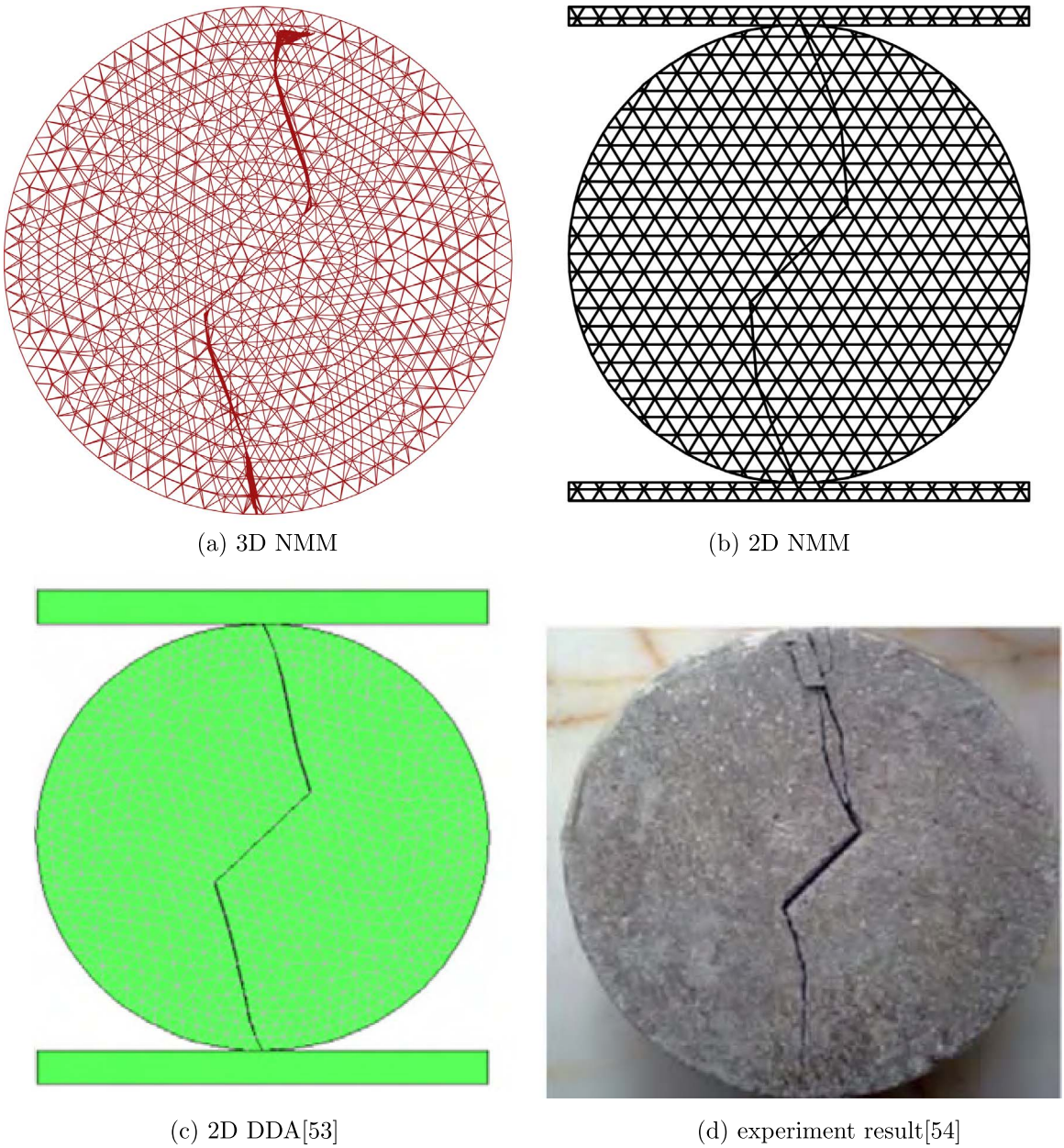

Fig. 14. The comparison between numerical simulation and experimental results for the fracture path of pre-notched disc ($\theta = 45°$), (a) 3D NMM (b) 2D NMM (c) 2D DDA [53] (d) experiment result [54].

components or structures, although it can well resolve the stress concentration near fracture tips and predict the possible propagations of existing fractures. Moreover, it is difficult for fracture mechanics to handle the complex fracture coalescences and intersections encountered in practical engineering problems [37]. In order to overcome the shortcoming of fracture mechanics, fracture algorithm based on strength criterion is utilized [37], which is named as Mohr-Coulomb criterion with a tensile cut-off. This strength criterion has successfully simulated typical mode-I and mode-II problems, as well as progressive failures of 2D rock slopes, where frictional contact of fracture surfaces is involved. As a preliminary exploration in 3D fracture propagation using NMM, we will not consider frictional contact of fracture surfaces and initiation of new fractures in this paper.

3.1. Maximum tensile stress criterion

The maximum tensile stress criterion has been widely used in rock mechanics because the parameters of this criterion can be conveniently determined by conventional uniaxial tensile test. Therefore, the maximum tensile stress criterion is employed in the 3D NMM for fracturing modeling in the present study.

The maximum tensile stress criterion can be written as

$$\sigma_1^{front} = T_0 \tag{10}$$

where T_0 is tensile strength of the material and σ_1^{front} is the maximum tensile stress of the fracture front. Once the maximum tensile stress exceeds the tensile strength T_0, the fracture front is advanced normal to the maximum tensile stress direction. It is noticed that the stress within each manifold element is constant because a tetrahedral mesh is used to generate the MC and constants are chosen as local approximations in the present paper. Weighted average of the stresses of all the manifold elements near the fracture front point is taken as the stress of a fracture front point, and expressed as

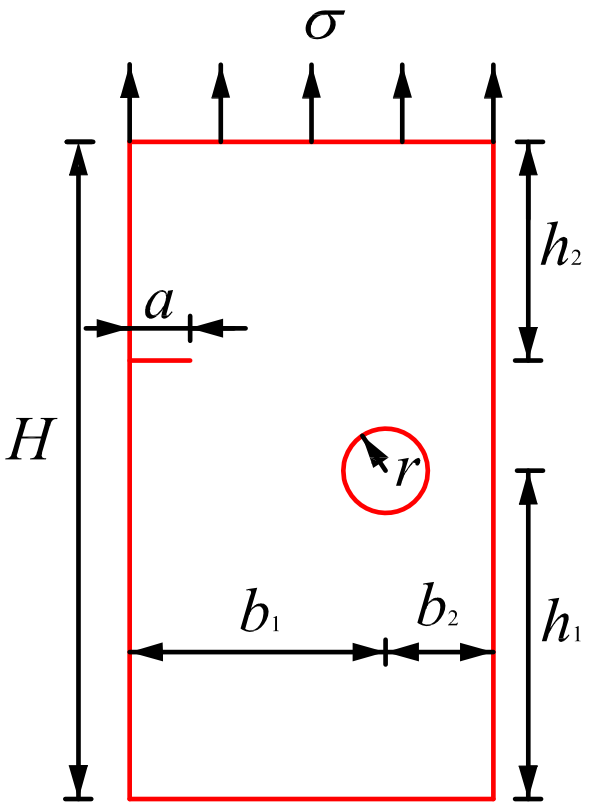

Fig. 15. A perforated plate with a circle hole subjected to a uniform tensile loading.

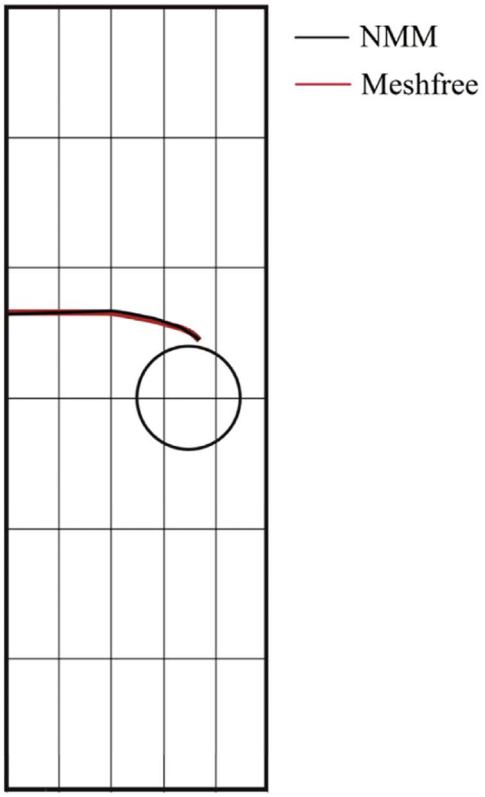

Fig. 17. The comparison of fracture paths within the perforated panel with a circular hole predicted obtained using 3D NMM and Meshfree method [56].

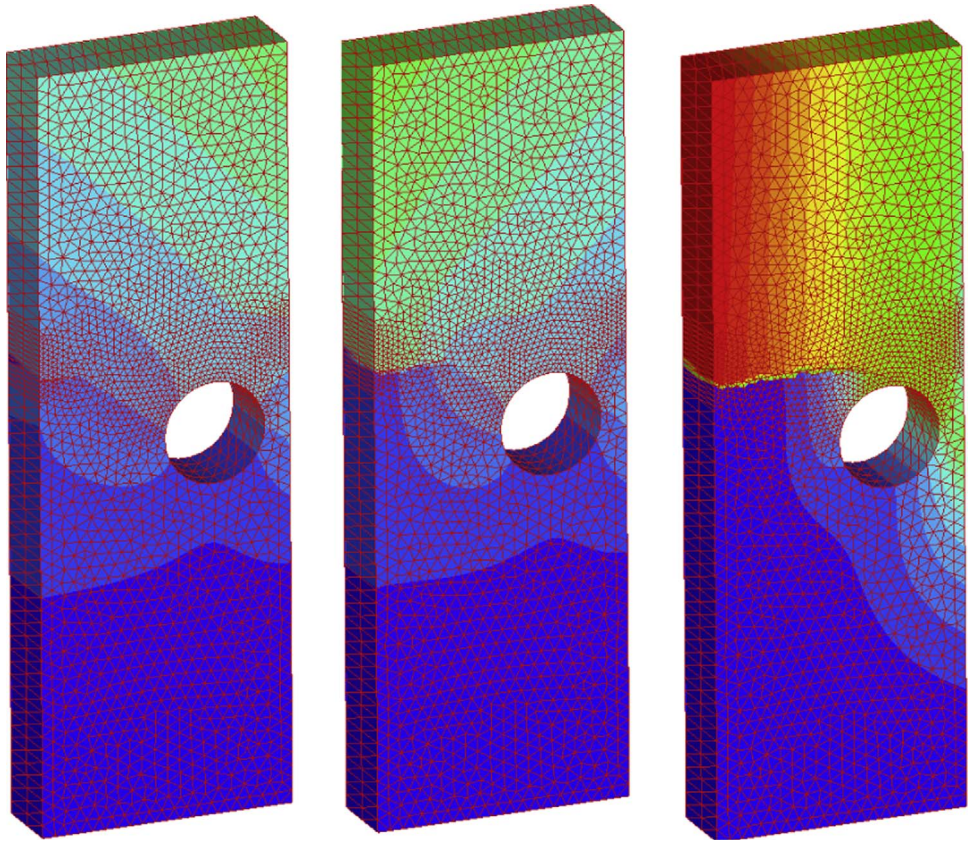

Fig. 16. The fracture path inside a perforated panel with a circular hole subjected to a uniform tensile loading with the 3D NMM.

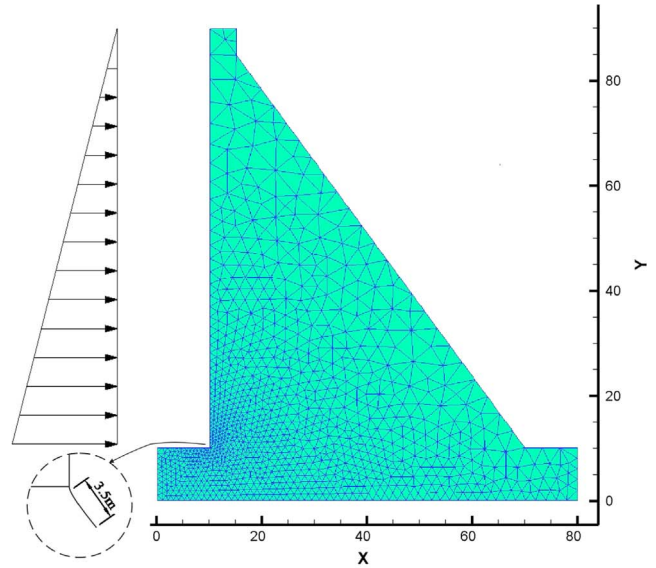

(a) geometry and boundary condition of dam and foundation

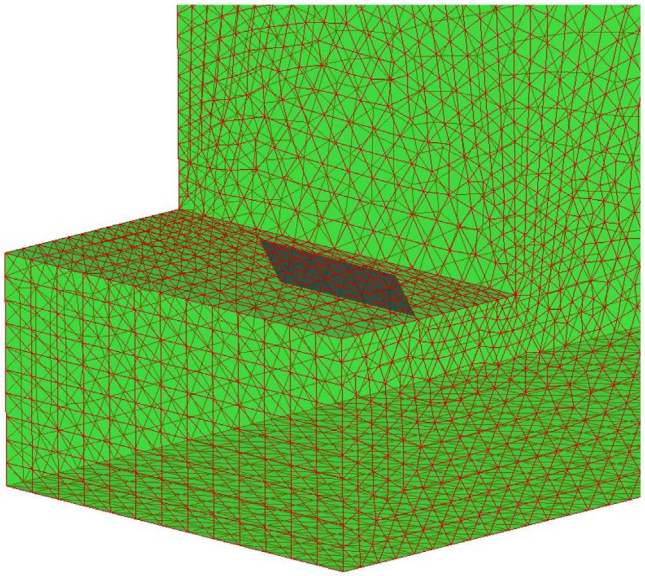

(b) the detial of initial penny crack

Fig. 18. Geometry and boundary condition.

Table 1
The evolution of the maximum principal stresses along fracture front.

Fracture length (m)	0.10	0.25	0.35	0.45
Maximum principal stresses (MPa)	0.2820	0.3192	0.3940	0.4835

$$\tilde{\boldsymbol{\sigma}}^{front} = \sum_{i=1}^{nmel} \varphi_i \hat{\boldsymbol{\sigma}}_i \tag{11}$$

where, *nmel* is the number of all the manifold elements near the fracture front point, $\hat{\boldsymbol{\sigma}}_i$ is the stress vector of *i*th manifold element and φ_i is the weight function, and expressed as

$$\varphi_i = \frac{L_i}{\sum_{j=1}^{nmel} L_j} \tag{12}$$

where

$$L_i = \frac{1}{d_i + \varepsilon} \tag{13}$$

where d_i is the distance from the center of *i*th manifold element to a fracture front point. ε is a very small, but positive number, and set to be 1.0^{-7} in the present work.

We also note that implementation of the fracture algorithm based on maximum tensile stress criterion is much easier, compared to the fracturing algorithm based on stress intensity factors.

3.2. Fracture trackings

The three dimensional fracture surface is mainly represented by segments or by other methods including level sets. In the level sets method applied to PU-based methods for three dimensional fracture problems [28,47,48], the fracture front vectors of the implicit representation of the fracture surface are computed based on the gradients of the front and surface level sets. However, this level set method may lead to an inaccurate representation of the fracture front because the orthogonality of the surface and front level set gradients does not always hold [48,49]. In this study, the fracture surface is represented by an explicit three dimensional triangulation.

Unlike Rabczuk et al. [50] using both triangular and quadrangular fracture cells to represent fracture surface, we only employ triangular fracture cell to fulfill the task for the purpose of simplicity. Shown in Fig. 5 is a schematic diagram of three dimensional triangular fracture cells representing fracture surface.

3.3. Topology update during fracturing process

Once the stress state at fracture front violates the maximum tensile stress criterion in Eq. (10), the old fracture front will advance to a new place. Some manifold elements which are near the old fracture front may be intersected. The intersection may result in manifold element with both regular and irregular shapes (Fig. 6).

In addition, some neighborong physical patches are split into two. Some other neighboring physical patches may be intersected. In each step, each physical patch is stored using its outer shell which consist of triangular cells. Here, each triangular cell consists of three points. It is noted that each physical patch corresponds to only one closed outer shell consisting of a series of closed loops, which is a generalization of two dimensional cases [38]. If the closed outer shell becomes two closed outer shells after cutting, then the target physical patch is split into two.

Since some physical patches and some manifold elements are altered, the physical patches for the related manifold elements must be updated. Assuming a physical patch $\{\Omega_i^p\}$ is partitioned into $\{\Omega_{i1}^p\}$ and $\{\Omega_{i2}^p\}$, updating the physical patches for the manifold elements can be fulfilled in two steps [37]. Firstly, all the manifold elements initially associated with the physical patch $\{\Omega_i^p\}$ should be found. Then, giving an arbitrary point within each manifold element, if this point is within $\{\Omega_{i1}^p\}$, $\{\Omega_{i1}^p\}$ is used to replace $\{\Omega_i^p\}$; if not, $\{\Omega_{i2}^p\}$ is used to replace $\{\Omega_i^p\}$.

3.4. Integration

In three-dimensional NMM, the manifold element, the basic unit in integrating the weak formulation of the problem, can be an arbitrarily shaped polyhedron [42]. Integration in NMM is usually undertaken explicitly using the simplex integration method [37]. The main advantage of simplex integration strategy over other integration strategies is its avoidance of element partitioning, which is usually adopted in other methods such as XFEM and GFEM to employ the numerical integration. Details implementation of the simplex integration method over arbitrarily shaped polyhedron can be found in [51].

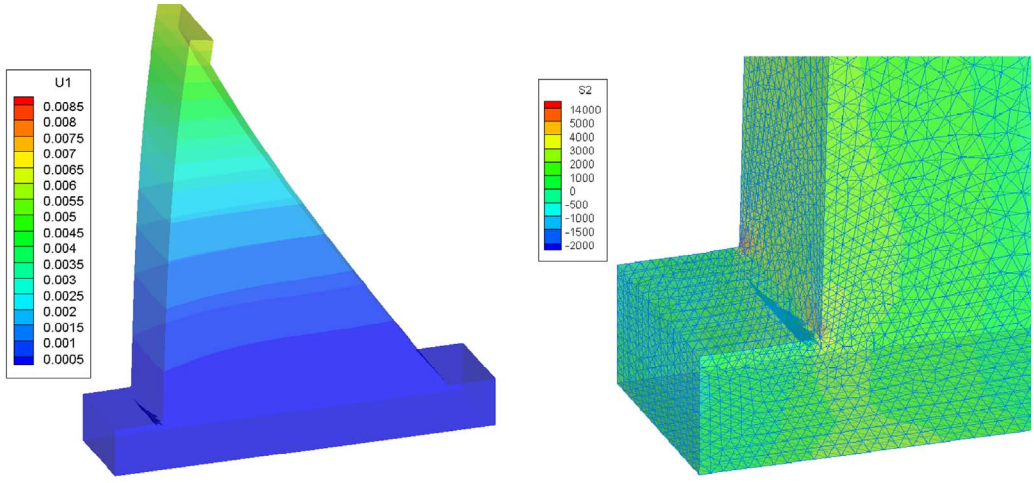

(a) displacement at step 2 (b) stress at step 2

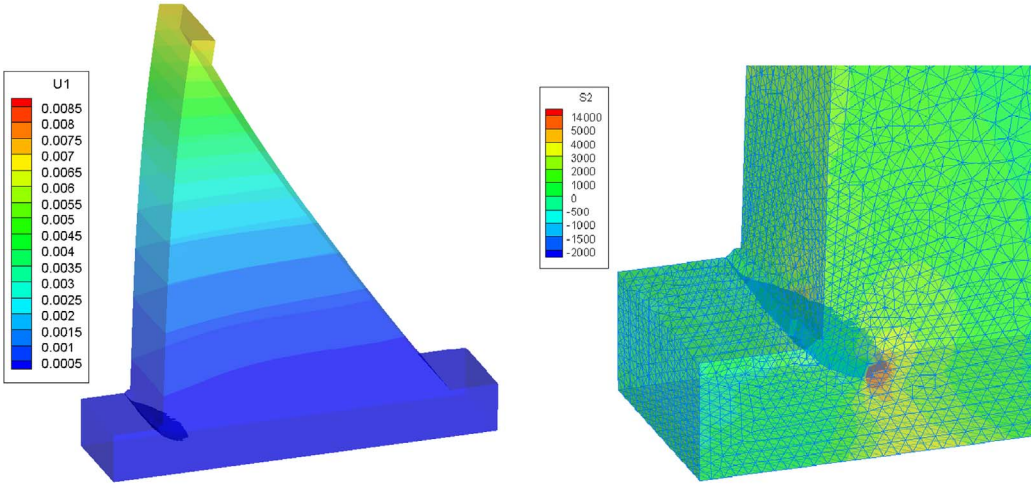

(c) displacement at step 4 (d) stress at step 4

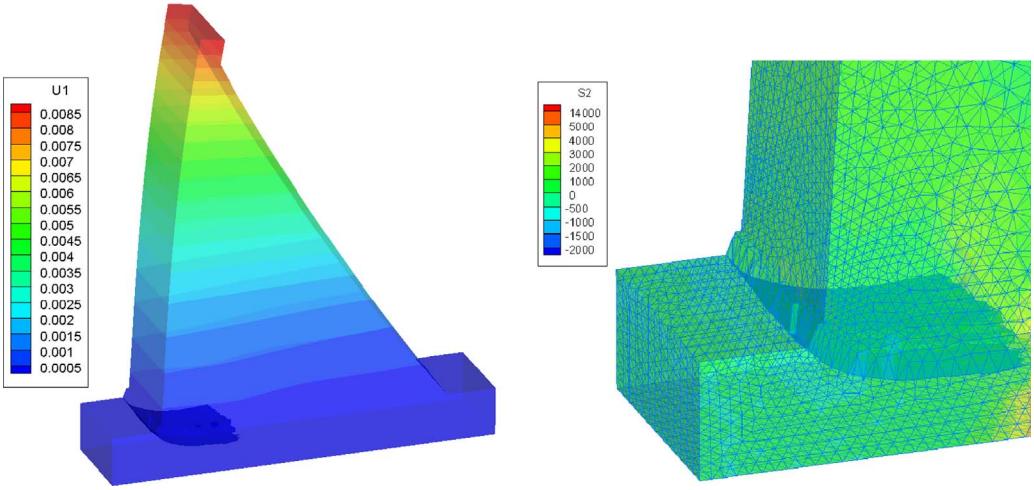

(e) displacement at step 8 (f) stress at step 8

Fig. 19. The fracture propagation at the base of a dam is shown, in which the domain containing fracture is amplified and shown in detail.

4. Numerical examples

Numerical tests for fracture propagation problems are carried out to show the validity and applicability of the present 3D NMM algorithm and code, which are discussed by comparing with numerical results and experimental results. Since the length of

fracture propagation used by the following examples is a constant, the fracture front may not stop at element boundaries. In the implementation, if the fracture front terminates inside manifold elements, this fracture front will be prolonged to the intersection between the boundaries of manifold elements and the extended fracture surface.

4.1. Beam under four-point loading

As the first example, a pre-notched beam subjected to four-point shear loading is studied, which is a classical experiment for structural engineering and is taken from Ref. [52]. The geometry and boundary conditions are shown in Fig. 7, with 4 m × 1 m × 0.4 m in geometry and load P=100 kPa. The material parameters are taken as Young's modulus $E = 1.0 \times 10^7$ MPa and Poisson's ratio $\nu = 0.3$. The length of fracture propagation at each computational step is constantly 0.15 m.

In this test, three models are calculated: 984 manifold elements with 3937 physical patches, 2465 manifold elements with 10,956 physical patches, and 5078 manifold elements with 23,265 physical patches. The process of fracture propagation with 23,265 physical patches is shown in Fig. 8. The fracture paths of three models are shown in Fig. 9(a), which are well consistent with that obtained in [9] using the Polygonal Finite Element Method (PFEM), see Fig. 9(b). As already stated in [9], it is again found in this work that fractures initially move away from each other, and finally propagate toward the loading points.

4.2. Fracture growth in a pre-notched disc

The brazilian test has been widely used in rock mechanics experiments to indirectly determine the tensile strength of rock-like brittle materials. As the second example for fracture propagation analysis, a circular cylindrical specimen with an central pre-existing fracture subjected to compressed loads along its diameter is considered, as shown in Fig. 10. In theory, the fractures should propagate towards to the location of loading points. The parameters in this computation are taken as, the diameter of the disc $D = 1$ m, Young's modulus $E = 1.0 \times 10^7$ MPa and Poisson's ratio $\nu = 0.3$. The length of fracture propagation at each computational step is 0.07 m.

In order to verify the stability and accuracy of 3D fracture propagation predicted by 3D NMM algorithm and code, two fracture inclination angles are studied, namely $\theta = 90^\circ$ (4299 manifold elements and 20,890 PPs) and $\theta = 45^\circ$ (4299 manifold elements and 20,890 PPs). The fracture propagation paths predicted with the present 3D NMM, 2D NMM, 2D DDA and experimental results are compared in Figs. 11–14. As expected, the propagation of the fracture path with 3D NMM is well consistent with those results predicted by 2D NMM, 2D DDA [53] and experimental results [54], as shown in Figs. 12 and 14.

4.3. Fracture growth in a perforated panel with a circular hole

As an example for fracture propagation, a perforated plate with a fixed bottom edge and subjected to a uniform tensile load at the top edge is considered, as shown in Fig. 15. This is a benchmark problem for fracture propagation, which has been studied in [55] using BEM, and in [56] using extended mesh free Galerkin radial point interpolation method (X-RPIM). Fig. 16(a) gives the mesh for this problem which consists of 8068 manifold elements and 35,435 physical patches. The parameters in the computation are taken as: $H = 3$ m; $h_1 = 1.5$ m; $h_2 = 1.2$ m; $b_1 = 0.7$ m; $b_2 = 0.3$ m; initial fracture length $a = 0.1$ m; $\sigma = 5$ kN/m^2, $E = 3.0 \times 10^4$ MPa, $\nu = 0.2$. The length of fracture propagation at each computational step is 1.7 m. The fracture growth paths obtained by the 3D NMM is shown in Fig. 16. As expected, the propagation of the fracture path is well consistent with that predicted by X-RPIM [56], see Fig. 17. As already stated in [55,56] and again found in this study that the fracture tip approaches the hole, it turns towards the hole and finally collapses with the hole (Fig. 18).

Table 1 shows the evolution of average maximum principal stresses at nodes along the fracture front. It is seen that the average maximum principal stresses increase with the growth of fracture length. In Ref. [55], the stress intensity factors increase with fracture length as well.

4.4. Fracture propagation inside a dam concrete foundation

As last example for fracture propagation, the fracture propagation inside a dam concrete foundation is modeled. The similar previous numerical tests can be found in references [57,58]. The geometry of the concrete dam and foundation are shown in Fig. 18 (a), which consists of 11681 manifold elements and 58,849 physical patches. The computational domain which consists of a penny crack is shown in detail in Fig. 18(b). The height of this dam is 80 m and overtopping water pressure is applied to the back of this concrete gravity dam. The length of fracture propagation at each computational step is 1.7 m. The material parameters in the computation are taken as: $E = 3.0 \times 10^4$ MPa, $\nu = 0.2$. Initially a penny crack is embedded inside the concrete dam foundation, which then grows and propagates to downstream. The process of fracture propagation is shown in Fig. 19, in which the computational domain containing fracture is amplified and shown in detail.

5. Discussion and conclusion

The concept of mathematical covers and physical covers is utilized in the Numerical Manifold Method (NMM), therefore it is able to handle displacement discontinuities in a straight forward manner without remeshing. Avoiding the difficulties of remeshing is significantly important for modeling the fracture propagation, especially for the analysis of 3D fracture propagation. Compared to 2D problems of fracture analysis, the geometry of 3D fractures is more complex, which is much more difficult to handle. In this paper, the fracture algorithm based on the maximum tensile stress criterion is utilized to determine the direction of 3D fracture propagation. In the numerical tests, four numerical tests are considered to validate the algorithm for 3D fracture propagation and NMM code. It has been shown that the present algorithm and 3D NMM code have the ability to accurately simulate 3D fracture propagation stably and effectively.

Since the present work is a preliminary exploration in the discontinuity modeling using 3D NMM, the advantages of 3D NMM, such as handling contact problems, have not been well revealed. In our following work, we will further enhance our algorithm and code to analyze complex and realistic rock mechanics problems in which multiple fracture initiation and propagation, tensile and shear fractures, and fracture propagations under compressive loading will be involved.

Acknowledgment

This research is supported by the National Basic Research Program of China (973 Program), under the Grant No. 2014CB046900 and 2015CB058100. This research is also supported by the Hubei Provincial Natural Science Foundation Project, under the Grant No. 2011CDA119.

References

[1] Lei Q, PaulLatham J, Xiang J, Tsang C. Polyaxial stress-induced variable aperture model for persistent 3d fracture networks. Geomech Energy Environ 2015;1:34–47.
[2] Zienkiewicz OC, Taylor RL. The Finite Element Method. Volume 1, The Basis, 5th ed., Butterworth-Heinemann; 2000.
[3] Gerstle W, Ingraffea A, Perucchio R. Three-dimensional fatigue fracture propagation analysis using the boundary element method. Int J Fatigue. 10, p. 187–92.
[4] Belytschko T, Krongauz Y, Organ D, Fleming M, Krysl P. Meshless methods: an overview and recent developments. Comput Methods Appl Mech Eng 1996;139(1–4):3–47.
[5] Moes N, Gravouil A, Belytschko T. Non-planar 3d fracture growth by the extended finite element and level sets - part I: mechanical model. Int J Numer Methods Eng 2014;53(11):2549–68.
[6] Manzini G, Russo A, Sukumar N. New perspectives on polygonal and polyhedral finite element methods. Math Models Methods Appl Sci 2014;24 (8):1665–99.
[7] Natarajana S, Ooib E, Chionga I, Songa C. Convergence and accuracy of displacement based finite element formulations over arbitrary polygons: laplace interpolants, strain smoothing and scaled boundary polygon formulation. Finite Elem Anal Des 2014;85:101–22.
[8] Krausa M, Rajagopal A, Steinmann P. Investigations on the polygonal finite element method: constrained adaptive delaunay tessellation and conformal interpolants. Comput Struct 2013;120:33–46.
[9] Tang X, Zheng C, Wu S, Zhang J. A novel virtual node method for polygonal elements. Appl Math Mech 2009;30(10):1233–46.
[10] Paluszny A, Zimmerman R. Numerical fracture growth modeling using smooth surface geometric deformation. Eng Fract Mech 2013;108:19–36.
[11] Tang X, Paluszny A, Zimmerman R. Energy conservative property of impulse-based methods for collision resolution. Int J Numer Methods Eng 2013;95 (6):529–40.
[12] Tang X, Paluszny A, Zimmerman R. An impulse-based energy tracking method for collision resolution. Comput Methods Appl Mech Eng 2014;278(15):160–85.
[13] Paluszny A, Tang X, Zimmerman R. A fracture- and impulse-based FDEM approach for fragmentation. Comput Mech 2013;52(5):1071–84.
[14] Iglauer S, Paluszny A, Blunt M. Erratum: simultaneous oil recovery and residual gas storage: a pore-level analysis using in situ X-ray micro-tomography. Fuel 2015;139:905–14.
[15] Iglauer S, Paluszny A, Blunt M. Simultaneous oil recovery and residual gas storage: a pore-level analysis using in situ x-ray micro-tomography. Fuel 2015;139 780–780.
[16] Lang P, Paluszny A, Zimmerman R. Permeability tensor of three-dimensional fractured porous rock and a comparison to tracemap predictions. J Geophys Res-Solid Earth 2014;119:6288–307.
[17] Blandford G, Ingraffea A, Liggett J. Two-dimensional stress intensity factor computations using the boundary element method. Int J Numer Methods Eng 1981;17(3):387–404.
[18] Wu K, Olson JE. Simultaneous multifracture treatments: fully coupled fluid flow and fracture mechanics for horiontal wells. SPE J 2015;20(2):337–46.
[19] Duarte C, Hamzeh O, Liszka T, Tworzydlo W. A generalized finite element method for the simulation of three dimensional dynamic crack propagation. Comput Methods Appl Mech Eng 2001;190(15–17):2227–62.
[20] Chen J, Pan C, Wu C, Liu W. Reproducing kernel particle methods for large deformation analysis of non-linear structures. Comput Methods Appl Mech Eng 1996;139(1–4):195–227.
[21] Rabczuk T, Belytschko T. Cracking particles: a simpli ed mesh-free method for arbitrary evolving cracks. Int J Numer Methods Eng 2004;61(13):2316–43.
[22] Belytschko T, Lu Y, Gu L. Element-free galerkin methods. Int J Numer Methods Eng 1994;37(2):229–56.
[23] Liu W, Jun S, Zhang Y. Reproducing kernel particle methods. Int J Numer Methods Fluids 1995;20(8–9):1081–106.
[24] Rabczuk T, Belytschko T, Xiao S. Stable particle methods based on lagrangian kernels. Comput Methods Appl Mech Eng 2004;193(26):1035–63.
[25] Bordas S, Rabczuk T, Zi G. Three-dimensional crack initiation, propagation, branching and junction in non-linear materials by an extended mesh-free method without asymptotic enrichment. Eng Fract Mech 2006;75(5):943–60.
[26] Zheng C, Wu S, Tang X, Zhang J. A novel twice-interpolation finite element method for solid mechanics problems. Acta Mech Sin 2010;26(2):265–78.
[27] Babuska I, Melenk JM. The partition of unity method. Int J Numer Methods Eng 1997;12:727–58.
[28] Gravouil A, Moes N, Belytschko T. Non-planar 3d crack growth by the extended finite element and level sets - part ii: Level set update. Int J Numer Methods Eng 2002;53(11):2569–86.
[29] Yu T, Bui T, Liu CZP, Hirose S. Interfacial dynamic impermeable cracks analysis in dissimilar piezoelectric materials under coupled electromechanical loading with the extended finite element method. Int J Solids Struct 2015;67–68:205–16.
[30] Strouboulis T, Babuka I, Copps K. The design and analysis of the generalized finite element method. Comput Methods Appl Mech Eng 2000;181(1–3):43–69.
[31] Zhang H, Li L, An X, Ma G. Numerical analysis of 2-D crack propagation problems using the numerical manifold method. Eng Anal Bound Elem 2010;34:41–50.
[32] Shi G, Manifold method of material analysis. In: Proceedings of the transcations of the Ninth Army Confernece on Applied Mathematics and Computing; 1991.
[33] Chiou Y, Lee Y, Tsay R. Mixed mode fracture propagation by manifold method. Int J Fract 2002;114:327–47.
[34] Terada K, Ishii T, Kyoya T, Kishino Y. Finite cover method for progressive failure with cohesive zone fracture in heterogeneous solids and structures. Comput Mech 2007;39:191–210.
[35] Zheng H, Liu F, Du X. Complementarity problem arising from static growth of multiple cracks and mls-based numerical manifold method. Comput Methods Appl Mech Eng 2015;295:150–71.
[36] Ma G, An X, Zhang H, Li L. Modelling complex crack problems using the numerical manifold method. Int J Fract 2009;156:21–35.
[37] Ning Y, An X, Ma G. Footwall slope stability analysis with the numerical manifold method. Int J Rock Mech Min Sci 2011;48:964–75.
[38] Wu Z, Wong L, Fan L. Dynamic study on fracture problems in viscoelastic sedimentary rocks using the numerical manifold method. Rock Mech Rock Eng 2013;46:1415–27.
[39] Zhang H, Ma G, Ren F. Implementation of the numerical manifold method for thermo-mechanical fracture of planar solids. Eng Anal Bound Elem 2014;44:45–54.
[40] Zheng H, Xu D. New strategies for some issues of numerical manifold method in simulation of crack propagation. Int J Numer Methods Eng 2014;97 (13):986–1010.
[41] He L, An X, Ma G, Zhao Z. Development of three-dimensional numerical manifold method for jointed rock slope stability analysis. Int J Rock Mech Min Sci 2013;64:22–35.
[42] Jiang Q, Zhou C, Li D. A three-dimensional numerical manifold method based on tetrahedral meshes. Comput Struct 2009;87:880–9.
[43] Yang Y, Tang X, Zheng H. A three-node triangular element with continuous nodal stress. Comput Struct 2014;141:46–58.
[44] Yang Y, Bi R, Zheng H. A hybrid fe-meshless quad4 with continuous nodal stress using radial-polynomial basis functions. Eng Anal Bound Elem 2015;53:73–85.
[45] Williams M. On the stress distribution at the base of a stationary crack. J Appl Mech 1957;24:109–14.
[46] He L, Ma G. Development of 3d numerical manifold method. Int J Comput Methods 2010;7:107–29.
[47] Sukumar N, Chopp D, Moran B. Extended finite element method and fast marching method for three-dimensional fatigue crack propagation. Eng Fract Mech 2003;70(1):29–48.
[48] Sukumar N, Moes N, Moran B, Belytschko T. Extended finite element method for three-dimensional crack modelling. Int J Numer Methods Eng 2000;48:1549–70.
[49] Pereira J, Duarte C, Jiao X, Guoy D. Generalized finite element method enrichment functions for curved singularities in 3d fracture mechanics problems. Comput Mech 2009;44:73–92.
[50] Rabczuk T, Bordas S, Zi G. A three-dimensional meshfree method for continuous multiple-crack initiation, propagation and junction in statics and dynamics. Comput Mech 2007;40:473–95.
[51] Shi G. Simplex integration for manifold method, fem, dda and analytical analysis. In: Proceedings of the first international forum on discontinuous deformation analysis (DDA) and simulations of discontinuous media, Albuquerque, p. 205–62.
[52] Bouchard P, Bay F, Chastel Y, Tovena I. Crack propagation modelling using an advanced remeshing technique. Comput Methods Appl Mech Eng. 189 (723–742).
[53] Ning Y, Yang J, An X, Ma G. Modelling rock fracturing and blast-induced rock mass failure via advanced discretisation within the discontinuous deformation analysis framework. Comput Geotech 2011;38:40–9.
[54] Haeri H, Shahriar K, Marji M, Moarefvand P. Experimental and numerical study of crack propagation and coalescence in pre-cracked rock-like disks. Int J Rock Mech Min Sci 2014;67:20–8.
[55] Leonel D, Venturini S. Multiple random crack propagation using a boundary element formulation. Eng Fract Mech 2011;78:1077–90.
[56] Nguyen N, Bui T, Zhang C, Truong T. Crack growth modeling in elastic solids by the extended meshfree galerkin radial point interpolation method. Eng Anal Bound Elem 2014;44:87–97.
[57] Secchi S, Schrefler B. A method for 3-d hydraulic fracturing simulation. Int J Fract 2012;178(1–2):245–58.
[58] Schrefler B, Secchi S, Simoni L. On adaptive refinement techniques in multi-field problems including cohesive fracture. Comput Methods Appl Mech Eng 2006;195(4–6):444–61.